Renormalization of local quark-bilinear operators for $N_f = 3$ flavors of stout link nonperturbative clover fermions

M. Constantinou,[1] R. Horsley,[2] H. Panagopoulos,[1] H. Perlt,[3] P. E. L. Rakow,[4] G. Schierholz,[5] A. Schiller,[3] and J. M. Zanotti[6]

[1]*Department of Physics, University of Cyprus, Nicosia CY-1678, Cyprus*
[2]*School of Physics and Astronomy, University of Edinburgh, Edinburgh EH9 3FD, United Kingdom*
[3]*Institut für Theoretische Physik, Universität Leipzig, 04103 Leipzig, Germany*
[4]*Theoretical Physics Division, Department of Mathematical Sciences, University of Liverpool, Liverpool L69 3BX, United Kingdom*
[5]*Deutsches Elektronen-Synchrotron DESY, 22603 Hamburg, Germany*
[6]*CSSM, School of Chemistry and Physics, University of Adelaide, Adelaide SA 5005, Australia*

(Received 2 September 2014; published 9 January 2015)

The renormalization factors of local quark-bilinear operators are computed nonperturbatively for $N_f = 3$ flavors of stout link nonperturbative clover (SLiNC) fermions, with emphasis on the various procedures for the chiral and continuum extrapolations. The simulations are performed at a lattice spacing $a = 0.074$ fm, and for five values of the pion mass in the range of 290–465 MeV, allowing a safe and stable chiral extrapolation. Emphasis is given in the subtraction of the well-known pion pole which affects the renormalization factor of the pseudoscalar current. We also compute the inverse propagator and the Green's functions of the local bilinears to one loop in perturbation theory. We investigate lattice artifacts by computing them perturbatively to second order as well as to all orders in the lattice spacing. The renormalization conditions are defined in the RI′-MOM scheme, for both the perturbative and nonperturbative results. The renormalization factors, obtained at different values of the renormalization scale, are translated to the $\overline{\text{MS}}$ scheme and are evolved perturbatively to 2 GeV. Any residual dependence on the initial renormalization scale is eliminated by an extrapolation to the continuum limit. We also study the various sources of systematic errors. Particular care is taken in correcting the nonperturbative estimates by subtracting lattice artifacts computed to one-loop perturbation theory using the same action. We test two different methods, by subtracting either the $\mathcal{O}(g^2a^2)$ contributions, or the complete (all orders in a) one-loop lattice artifacts.

DOI: 10.1103/PhysRevD.91.014502 PACS numbers: 11.15.Ha, 11.10.Gh, 11.15.Bt, 12.38.Gc

I. INTRODUCTION

To make contact between lattice QCD simulation results and phenomenological numbers, which usually are given in the $\overline{\text{MS}}$ scheme, we need to compute renormalization factors relating the bare lattice operators to renormalized ones. This requires a nonperturbative method, because low-order lattice perturbation theory is unreliable at present couplings. One such method is the regularization independent momentum (RI-MOM) renormalization scheme [1], which mimics the renormalization procedure used in continuum perturbation theory. In practical applications a variant of the RI-MOM scheme is preferred, the so-called RI′-MOM scheme, which differs from the RI-MOM scheme only in the quark field renormalization factor. The results can be converted to the $\overline{\text{MS}}$ scheme using continuum perturbation theory.

The method involves comparing lattice calculations of off-shell Green's functions with continuum perturbation theory results. This matching will work best at large virtualities or short distances, where the running coupling constant is small, and the effects of nonperturbative phenomena, such as chiral symmetry breaking, have died away. A drawback of the method is that discretization effects grow rapidly at short distances. It is thus desirable to remove the discretization errors in the off-shell lattice Green's functions before making the comparison with the continuum.

The fact that chiral symmetry is broken on the lattice requires special attention as compared to continuum treatments. In particular, renormalization constants for the vector (scalar) operator will not coincide with those of the axial vector (pseudoscalar) one; however, no mixing will occur among the operators which we are considering here.

Two approaches have been pursued. In [2] the full one-loop perturbative correction has been subtracted from the Green's functions for operators with up to one covariant derivative, for the plaquette action and $N_f = 2$ flavors of clover fermions. This procedure becomes very elaborate for higher dimensional operators and more complex actions. An alternative approach is to restrict oneself to one-loop corrections of $O(a^2)$. The relevant expressions have been computed in [3] for a variety of operators and actions. In [4] we have compared the results of both methods using the Wilson action; we found agreement for that action to be

better than 1% for local operators and better than 2% for operators with one covariant derivative.

In this work we compute renormalization factors for $N_f = 3$ flavors of SLiNC (stout link nonperturbative clover) fermions [5,6] and local quark-bilinear operators, studying the effects of one-loop $O(a^2)$ subtraction, as well as the complete subtraction to one loop. The particular clover action used here has a single iterated mild stout smearing for the hopping terms, together with thin links for the clover term. For the gauge fields we are using the tree-level Symanzik action. Although we present different approaches to improve our nonperturbative estimates, for our final results we adopt the complete subtraction of the one-loop lattice artifacts with boosted coupling g_b. The stout-link improved action employed here, appears to suppress lattice artifacts in quark Green's functions since it leads to smaller lattice artifacts compared to the non-smeared case.

The paper is organized as follows: In Sec. II we explain our method of nonperturbative renormalization and its numerical implementation, along with the data sets used in this work and a precise determination of the lattice scale. In Sec. III we briefly outline our perturbative computation and the different methods of subtraction. Then, in Sec. IV we present our nonperturbative results in the RI′-MOM scheme, the chiral extrapolation and the conversion to the $\overline{\text{MS}}$ scheme. The continuum extrapolation appears in Sec. V, where in Sec. V A we give our final nonperturbative estimates in the schemes $\overline{\text{MS}}$ at 2 GeV, renormalization group invariant (RGI), and RI′-MOM at a scale of 1/a. The quality of the data upon subtraction of the perturbative terms is demonstrated in Sec. V B, and finally, in Sec. VI we present our final results and conclude. We also include three appendixes: A: a summary of our perturbative results; B: the β-function and anomalous dimensions that are necessary for the conversion to the $\overline{\text{MS}}$ and RGI schemes; and C: an alternative fitting for the pion pole subtraction.

II. METHOD AND NUMERICAL IMPLEMENTATION

The operators which we study in this paper are listed in Table I, along with their representations under the hypercubic group $H(4)$ [7]. We work on lattices with spacing a and volume V, gauge fixed to Landau gauge. Starting from the Green's function

$$G_{\alpha\beta}(p) = \frac{a^{12}}{V}\sum_{x,y,z} e^{-ip\cdot(x-y)}\langle q_\alpha(x)\mathcal{O}(z)\bar{q}_\beta(y)\rangle, \quad (1)$$

$q = u, d$ or s, with operator insertion $\mathcal{O}$, we obtain the vertex function (or amputated Green's function)

$$\Gamma(p) = S^{-1}(p)G(p)S^{-1}(p), \quad (2)$$

where

$$S_{\alpha\beta}(p) = \frac{a^8}{V}\sum_{x,y} e^{-ip\cdot(x-y)}\langle q_\alpha(x)\bar{q}_\beta(y)\rangle \quad (3)$$

denotes the quark propagator. Following [1,2,4] we define the renormalized vertex function by

$$\Gamma_{\text{R}}(p) = Z_q^{-1} Z\Gamma(p) \quad (4)$$

and fix the renormalization factor Z by imposing the renormalization condition

$$\frac{1}{12}\text{Tr}[\Gamma_{\text{R}}(p)\Gamma^{-1}_{\text{Born}}(p)]_{p^2=\mu^2} = 1, \quad (5)$$

where μ is the renormalization scale. The renormalization function of the fermion field ($q_R = Z_q q$) is given by

$$\begin{aligned} Z_q(\mu) &= \Lambda_q(p)|_{p^2=\mu^2}, \\ \Lambda_q(p) &= \frac{\text{Tr}(-i\sum_\lambda \gamma_\lambda \sin(ap_\lambda) a S^{-1}(p))}{12\sum_\lambda \sin^2(ap_\lambda)} \end{aligned} \quad (6)$$

where $\Lambda_q(p)$ is the projection of the fermion propagator onto the tree-level or Born massless quark propagator. The renormalization factor Z is calculated from the condition

$$Z_q^{-1} Z\,\Lambda(p)|_{p^2=\mu^2} = 1, \qquad \Lambda(p) = \frac{1}{12}\text{Tr}[\Gamma(p)\Gamma^{-1}_{\text{Born}}(p)] \quad (7)$$

where $\Lambda(p)$ is the projected amputated Green's function and $\Gamma_{\text{Born}}(p)$ is the Born term of the vertex function. Finally, Z has to be extrapolated to the chiral limit. Note that Eq. (7) is not afflicted with $O(a)$ lattice artifacts, which are associated with operators of opposite chirality and drop out when the trace is taken.

The calculations are done for five sets of mass-degenerate quarks, $m_u = m_d = m_s$, on $32^3 \times 64$ lattices at $\beta = 5.50$ [6], with the SLiNC action. The clover parameter, c_{sw}, was set to 2.65, and the stout parameter, ω to 0.1 [5]. The ω is involved in the definition of the stout smeared link:

TABLE I. The operators under study and their representations under the hypercubic group H(4) [7].

Operator	Lorentz structure	Representation	Operator basis
$\mathcal{O}^S$	$\bar{q}q$	$\tau_1^{(1)}$	$\mathcal{O}^S$
$\mathcal{O}^P$	$\bar{q}\gamma_5 q$	$\tau_1^{(1)}$	$\mathcal{O}^P$
$\mathcal{O}^V_\mu$	$\bar{q}\gamma_\mu q$	$\tau_1^{(4)}$	$\mathcal{O}^V_1, \mathcal{O}^V_2, \mathcal{O}^V_3, \mathcal{O}^V_4$
$\mathcal{O}^A_\mu$	$\bar{q}\gamma_\mu\gamma_5 q$	$\tau_1^{(4)}$	$\mathcal{O}^A_1, \mathcal{O}^A_2, \mathcal{O}^A_3, \mathcal{O}^A_4$
$\mathcal{O}^T_{\mu\nu}$	$\bar{q}\sigma_{\mu\nu} q$	$\tau_1^{(6)}$	$\mathcal{O}^T_{12}, \mathcal{O}^T_{13}, \mathcal{O}^T_{14}, \mathcal{O}^T_{23}, \mathcal{O}^T_{24}, \mathcal{O}^T_{34}$

TABLE II. Parameters κ_l ($l = u, d$), κ_s and pion masses of our lattice ensembles at $\beta = 5.50$.

κ_ℓ	κ_s	am_π
0.120900	0.120900	0.1757(10)
0.120920	0.120920	0.1647(4)
0.120950	0.120950	0.1508(4)
0.120990	0.120990	0.1285(7)
0.121021	0.121021	0.1089(21)

$$\tilde{U}_\mu = \exp\{\mathrm{i}Q_\mu(x)\}U_\mu(x),$$
$$Q_\mu(x) = \frac{\omega}{2\mathrm{i}}[VU^\dagger - UV^\dagger - \frac{1}{3}\mathrm{Tr}(VU^\dagger - UV^\dagger)], \quad (8)$$

where V_μ is the sum of all staples around U_μ. We note that as in Ref. [5] the clover term is built from the usual links. The parameters of the corresponding gauge field configurations are listed in Table II. In terms of the hopping parameter κ_q, the quark masses are given by

$$am_q = \frac{1}{2\kappa_q} - \frac{1}{2\kappa_{0c}} \quad (9)$$

with $\kappa_{0c} = 0.121099(3)$. We use momentum sources [8] to compute the Green's functions of Eq. (1) and discard quark-line disconnected contributions. Thus, unless stated otherwise, our renormalization factors refer to flavor nonsinglet operators. The momentum source method samples over all lattice points rather than only a few in the original approach. In this work we use 10 configurations on each ensemble which prove to be sufficient. These configurations were produced in trajectories of $\mathcal{O}(2000)$ sweeps, with measurements every 200 trajectories. The independence of these configurations has been checked by calculating, using the Wilson flow, the autocorrelation function for the topological charge, which corresponds to the slowest modes. To convert the renormalization factors to physical scales μ, we need to know the lattice spacing a. We consider extrapolations to the physical point from a point on the $SU(3)$ flavor symmetric line by keeping the average quark mass $\bar{m} = (m_u + m_d + m_s)/3$ fixed. With this condition flavor singlet quantities turn out to be flat in $\delta m_q = m_q - \bar{m}$ up to corrections of $O(\delta m_u^2 + \delta m_d^2 + \delta m_s^2)$ [6]. Let us briefly mention our strategy to determine the scale using singlet quantities, which we collectively denote by X_S. We consider X_π, X_ρ and X_N, the center of mass of the pseudoscalar meson, vector meson, and baryon octet [with $X_\pi^2 = (M_{K^+}^2 + M_{K^0}^2 + M_{\pi^+}^2 + M_{\pi^-}^2 + M_{\bar{K}^0}^2 + M_{K^-}^2)/6$, and similarly for ρ and N], as well as the pure gluon quantities $X_{t_0} = 1/\sqrt{t_0}$ and $X_{w_0} = 1/w_0$ based on the Wilson gauge flow [9,10]. Knowing X_S^{exp}, this enables us to determine the lattice spacing for the individual singlets by

$$a_S^2 = \frac{(a_S X_S)^2}{X_S^{\mathrm{exp}\,2}}. \quad (10)$$

The $SU(3)$ flavor symmetric point is marked by the hopping parameter κ_0. We can locate κ_0 by finding a point where we have a common scale [11]. In Fig. 1 we plot a_S^2 against $1/\kappa_0$, where the crossing of a_S^2 for $S = \pi$, ρ and N give an estimate of the common scale $a = 0.074(2)$ fm. We can now adjust X_{t_0} and X_{w_0} to also cross at this point, which gives $\sqrt{t_0}^{\mathrm{exp}} = 0.153(7)$ fm and $w_0^{\mathrm{exp}} = 0.179(6)$ fm. With this choice of the lattice spacing, the pion masses in Table II range from 290 to 465 MeV, allowing a controlled extrapolation to the chiral limit. The renormalization factors are converted to the $\overline{\mathrm{MS}}$ scheme at $\mu = 2$ GeV.

The lattice momenta are chosen according to

$$\Lambda_{\mathrm{QCD}}^2 \ll p^2 \leq \left(\frac{\pi}{a}\right)^2. \quad (11)$$

On $L^3 \times T$ lattices with periodic spatial and antiperiodic temporal boundary conditions

$$p = \left(\frac{2\pi}{L}n_1, \frac{2\pi}{L}n_2, \frac{2\pi}{L}n_3, \frac{2\pi}{T}\left(n_4 + \frac{1}{2}\right)\right). \quad (12)$$

To increase the number of momenta, we employ twisted boundary conditions to the quark fields, $p \to p + B$, with

$$B = \left(\frac{2\pi}{L}\theta_1, \frac{2\pi}{L}\theta_2, \frac{2\pi}{L}\theta_3, \frac{2\pi}{T}\theta_4\right). \quad (13)$$

Thus for lattices with $T = 2L$ then

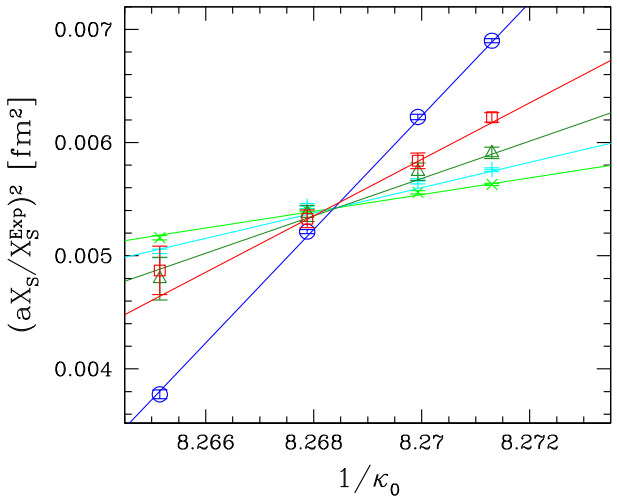

FIG. 1 (color online). The lattice spacing a_S for $S = \pi$ (○), ρ (△), N (□), t_0 (×), and w_0 (+).

TABLE III. Lattice momenta and twist angles in lattice units.

$\theta = (0,0,0,-\frac{1}{2})$		$\theta = (\frac{1}{2},\frac{1}{2},\frac{1}{2},-\frac{1}{2})$		$\theta = (\frac{1}{4},\frac{1}{4},\frac{1}{4},0)$	
n	$(a\,p)^2$	n	$(a\,p)^2$	n	$(a\,p)^2$
(1, 1, 1, 2)	0.1542	(0, 0, 0, 1)	0.03855	(0, 0, 0, 0)	0.009638
(2, 2, 2, 4)	0.6169	(1, 1, 1, 3)	0.3470	(1, 1, 1, 2)	0.2410
(3, 3, 3, 6)	1.3879	(2, 2, 2, 5)	0.9638	(2, 2, 2, 4)	0.7807
(4, 4, 4, 8)	2.4674	(3, 3, 3, 7)	1.8891	(3, 3, 3, 6)	1.6289
(5, 5, 5, 10)	3.8553	(4, 4, 4, 9)	3.1228	(4, 4, 4, 8)	2.7855
(6, 6, 6, 12)	5.5517	(5, 5, 5, 11)	4.6649	(5, 5, 5, 10)	4.2505
(7, 7, 7, 14)	7.5564	(6, 6, 6, 13)	6.5155	(6, 6, 6, 12)	6.0239
(8, 8, 8, 16)	9.8696	(7, 7, 7, 15)	8.6745	(7, 7, 7, 14)	8.1058

$$p = \frac{2\pi}{L}\left(n_1+\theta_1, n_2+\theta_2, n_3+\theta_3, \frac{1}{2}\left(n_4+\frac{1}{2}+\theta_4\right)\right). \tag{14}$$

We choose a fixed direction and then let p^2 vary. The optimal choice is along the diagonal ($p_1 = p_2 = p_3 = p_4$), which leaves us with overall $O((ap)^2)$ corrections only, but no directional correction [12]. Our momenta and twist angles are listed in Table III.

III. PERTURBATIVE ESTIMATION OF LATTICE ARTIFACTS

Our perturbative computation for the renormalization factors is performed in one-loop perturbation theory using a variety of fermionic and gluonic actions. In this paper we focus on the SLiNC action [13] providing the results for general gauge, α, [$\alpha = 0(1)$ for Landau (Feynman) gauge] and action parameters ($c_{\rm sw}, \omega$). The Feynman diagrams entering this computation and the procedure for their evaluation are extensively described in Ref. [14]. For comparison with the nonperturbative renormalization factors, in the results shown in this section we employ $\omega = 0.1$ for the parameter appearing in the stout links of the fermion part, and for the clover parameter we test both the tree-level value suggested by one-loop perturbation theory, $c_{\rm sw} = 1$ and the value employed in the simulations, that is [5]: $c_{\rm sw} = 2.65$. We have performed two separate computations to one loop, as described below:

(A) up to second order in the lattice spacing, a, for which the results are given in a closed form as a function of the external momentum p and well as a, α, $c_{\rm sw}$ and ω;

(B) to all orders in a, for general values of a, α, $c_{\rm sw}$ and ω, but for specific choices for the external momentum; we have computed these terms for all the momenta employed in the nonperturbative computation.

Our results for each computation are discussed below.

A. Subtraction of $\mathcal{O}(g^2a^2)$ contributions

We compute to one loop the inverse propagator, $S^{-1}(p)$, and the amputated two-point Green's functions of the local operators (scalar, pseudoscalar, vector, axial-vector, tensor), $\Gamma_{\mathcal{O}}(p)$. The Z-factors are extracted by applying the renormalization conditions given in Eqs. (6) and (7). The tree-level values for the fermion operators $\mathcal{O} = S, P, V, A$ and T are

$$\Gamma_{\rm Born}(p) = -i\mathbb{1},\ -i\gamma_5,\ -i\gamma_\mu,\ -i\gamma_5\gamma_\mu,\ -i\gamma_5\sigma_{\mu\nu}, \tag{15}$$

respectively. In the mass-independent schemes which we consider, the bare quark masses must be set to zero. Renormalization factors are defined in a way as to render Green's functions finite and to respect a given renormalization condition in the $a \to 0$ limit; that is, contributions of higher order in a are absent from the definition of Z's. Thus, omitting $\mathcal{O}(g^2a^2)$ terms from the Green's function entering Eqs. (6) and (7), we obtain

$$Z_q = 1 + \frac{g^2 C_F}{16\pi^2}(-13.0233 + 4.79201\alpha + c_{\rm sw}(2.01543 - 4.67344\omega) + 1.24220c_{\rm sw}^2 + 152.564\omega - 541.381\omega^2 - \alpha\log(a^2\mu^2)), \tag{16}$$

$$Z_S = 1 + \frac{g^2 C_F}{16\pi^2}(-13.6067 - \alpha + c_{\rm sw}(18.2213\omega - 6.83528) + 1.36741c_{\rm sw}^2 + 140.264\omega - 481.361\omega^2 + 3\log(a^2\mu^2)), \tag{17}$$

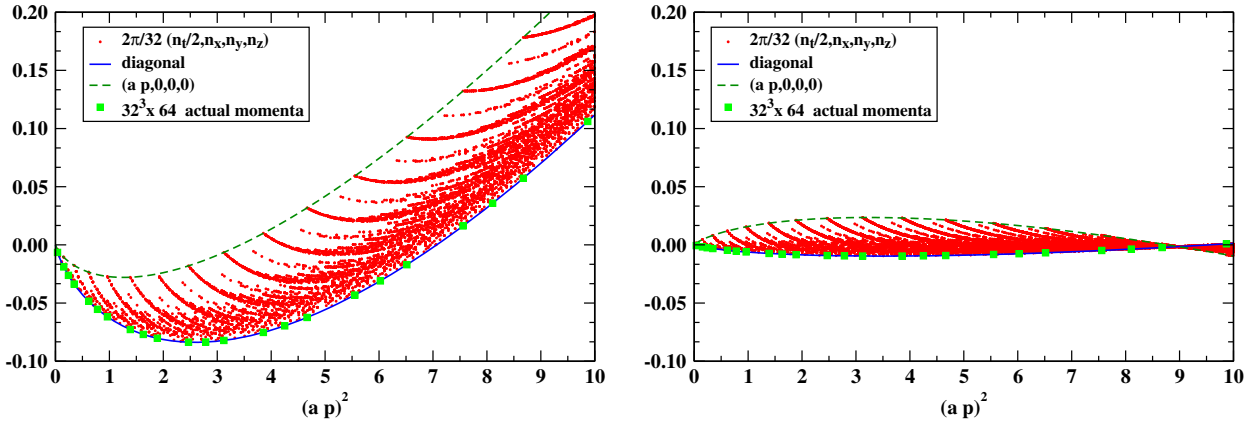

FIG. 2 (color online). $\Lambda_q^{(2)}$ as a function of $(a\,p)^2$ for $\omega = 0.1$ and (i) $c_{\rm sw} = 2.65$ (left); (ii) $c_{\rm sw} = 1$ (right). For comparison, to one loop: $Z_q = 1.14807$ for $c_{\rm sw} = 2.65$ and $Z_q = 0.99401$ for $c_{\rm sw} = 1$.

$$Z_P = 1 + \frac{g^2 C_F}{16\pi^2}(-21.7334 - \alpha + c_{\rm sw}(2.01543 - 4.67344\omega) - 1.74485 c_{\rm sw}^2 + 201.198\omega - 649.867\omega^2 + 3\log(a^2\mu^2)), \tag{18}$$

$$Z_V = 1 + \frac{g^2 C_F}{16\pi^2}\left(-16.5029 + \frac{\alpha}{2} + c_{\rm sw}(4.2281 - 10.3971\omega) + 0.46414 c_{\rm sw}^2 + 168.263\omega - 584.846\omega^2\right), \tag{19}$$

$$Z_A = 1 + \frac{g^2 C_F}{16\pi^2}\left(-12.5396 + \frac{\alpha}{2} + c_{\rm sw}(1.05025\omega - 0.19725) + 2.02027 c_{\rm sw}^2 + 137.796\omega - 500.593\omega^2\right), \tag{20}$$

$$Z_T = 1 + \frac{g^2 C_F}{16\pi^2}(-13.5383 + \alpha + c_{\rm sw}(3.49054 - 8.48923\omega) + 1.71918 c_{\rm sw}^2 + 147.129\omega - 535.088\omega^2 - \log(a^2\mu^2)), \tag{21}$$

where $C_F = (N^2 - 1)/(2N)$.

The $\omega = 0$ terms in the results given in this paper have been computed for the work published in Ref. [4] for a variety of gluon actions (beyond the plaquette action employed in Ref. [4]), including the tree-level Symanzik action which is used here. For completeness, in the framework of the computation with the stout smearing we have extended our results to $\omega \neq 0$.

The $\mathcal{O}(g^2a^2)$ contributions of the Green's functions are useful in nonperturbative computations of the Z-factors, since they may be subtracted from the nonperturbative values. Unfortunately, these terms are reliable up to a limited range of the lattice spacing, for which we cannot have an estimate prior the computation. Our experience showed that the presence of the clover parameter leads to larger $\mathcal{O}(g^2a^2)$ terms, possibly due to the polynomial dependence of the latter on $c_{\rm sw}$ (see e.g., Fig. 4). Nevertheless, the investigation of the $\mathcal{O}(g^2a^2)$ terms is definitely interesting, since comparison with the complete one-loop lattice artifacts (see Sec. III B) reveals whether the $\mathcal{O}(g^2a^2)$ terms carry the majority of the artifacts or not. Finally, they also serve a cross-check purpose, because for small values of $(a\,p)^2$ their numerical values for given action parameters must be almost equivalent with the complete one-loop lattice artifacts, as shown in Figs. 5–7.

As an example we show the expression for the projected quark-antiquark Green's function Λ_q defined in Eq. (6):

$$\Lambda_q = Z_q + \Lambda_q^{(2)} \tag{22}$$

using tree-level Symanzik gluons, Landau gauge $c_{\rm sw} = 2.65$ and $\omega = 0.1$. The $\mathcal{O}(g^2a^0)$ contribution gives Z_q, while the $\mathcal{O}(g^2a^2)$ terms are denoted by $\Lambda_q^{(2)}$; the latter is given by

$$\Lambda_q^{(2)} = a^2 \frac{g^2 C_F}{16\pi^2}\left[p^2(-0.8825 + 0.3972\log(a^2p^2)) + \frac{p4}{p^2}\left(1.9141 - \frac{157}{180}\log(a^2p^2)\right)\right]. \tag{23}$$

Beyond $\mathcal{O}(a^0)$, the terms depend not only on the length, but also on the direction of the four-vector p, due to the appearance of the Lorentz noninvariant terms $p4 \equiv \sum_\rho p_\rho^4$.

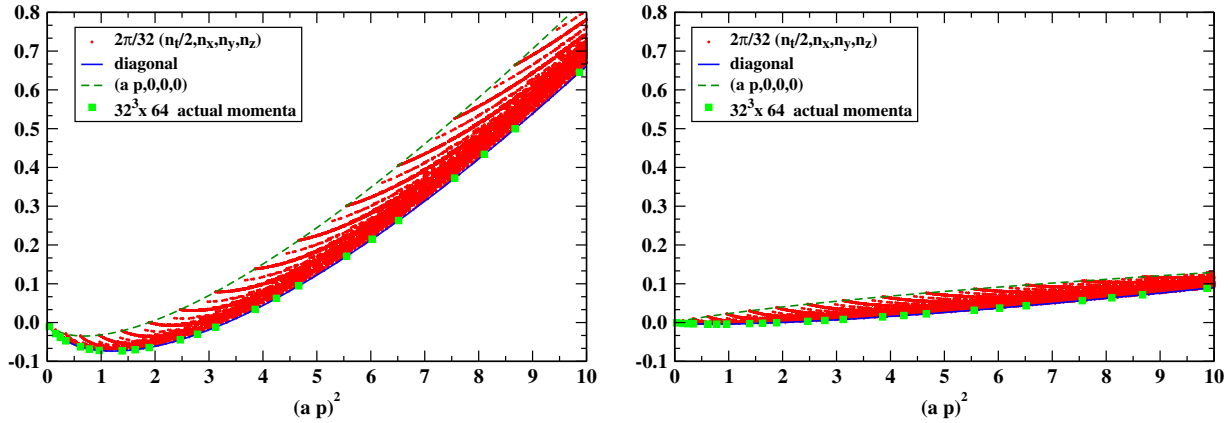

FIG. 3 (color online). Similar to Fig. 2 for $\Lambda_A^{(2)}$. For comparison, to one loop: $Z_A = 1.15623$ for $c_{\rm sw} = 2.65$ and $Z_A = 0.97179$ for $c_{\rm sw} = 1$.

In the left panel of Fig. 2 we plot $\Lambda_q^{(2)}$ of Eq. (23). In the figure we highlight (in green) the values of the momenta which we actually employ in the nonperturbative evaluation of the Z-factors. An immediate observation from the plot is that $\Lambda_q^{(2)}$ is significantly large (especially for the diagonal momenta) as compared to the one-loop perturbative estimate of Z_q at the same action parameters ($Z_q = 1.148$). This is in contrary to the case of $N_f = 2$ calculated for Wilson fermions and plaquette action, in which $c_{\rm sw} = 1$, and thus, to understand better the behavior of $\Lambda_q^{(2)}$ we plot it in the right panel of Fig. 2 for $c_{\rm sw} = 1$ and $\omega = 0.1$. Indeed, the $\mathcal{O}(g^2a^2)$ terms in this case are one order of magnitude smaller compared to the case of $c_{\rm sw} = 2.65$, and thus under control ($Z_q = 0.99401$ for $c_{\rm sw} = 1$). By analogy with Eq. (23) and Fig. 2, we also plot in Fig. 3 the $\mathcal{O}(g^2a^2)$ terms for Z_A, $\Lambda_A^{(2)}$ ($\Lambda_A \equiv Z_A + \Lambda_A^{(2)}$):

$$\Lambda_A^{(2)} = a^2 \frac{g^2 C_F}{16\pi^2}\left[p^2(-0.8337 + 0.5806\log(a^2p^2)) + \frac{p4}{p^2}\left(2.3481 - \frac{157}{180}\log(a^2p^2)\right)\right]. \quad (24)$$

In this case, the effect of $\Lambda_A^{(2)}$ on the one-loop perturbative value of $Z_A = 1.156$ is even more pronounced at $c_{\rm sw} = 2.65$. Another difference between the $N_f = 2$ and $N_f = 3$ cases is that in the latter the diagonal momenta do not lead to the smallest $\mathcal{O}(g^2a^2)$ effect. As a consequence, the pure nonperturbative data (estimated with diagonal momenta) and the $\mathcal{O}(a^2)$ subtracted data have a significant numerical difference. On the other hand, for Wilson fermions, the diagonal momenta lead to suppressed $\mathcal{O}(g^2a^2)$ effects; we had taken that observation on the $N_f = 2$ case as supporting evidence for the choice of diagonal momenta.

It is also interesting to investigate the $c_{\rm sw}$ dependence of $\Lambda_q^{(2)}$ for various values of $(a\,p)^2$. For this testing we set $\omega = 0.1$ and the dependence is shown in Fig. 4. The left panel corresponds to diagonal momenta (equal components), while the right panel to momenta with a nonzero component in a single direction. We observe that for $c_{\rm sw} < 1.5$ the $\mathcal{O}(g^2a^2)$ terms are very small, while for $c_{\rm sw} > 2$ these contributions increase very fast.

Although we have tested both $c_{\rm sw} = 1$ and $c_{\rm sw} = 2.65$, we choose to employ the tree-level value $c_{\rm sw} = 1$ for consistency to one-loop perturbation theory. This will be the value used in the subtraction of lattice artifacts from the nonperturbative estimates (Sec. V B).

A collection of the perturbative results for the $\mathcal{O}(g^2a^2)$ terms is given in Appendix A.

B. Complete subtraction of one-loop lattice artifacts

Here we present our results for the one-loop computation including all orders in the lattice spacing. The main motivation for such a calculation comes from the observation that at high values of $(a\,p)^2$ the $\mathcal{O}(g^2a^2)$ terms are no longer under control and become large. This does not necessarily indicate large artifacts, since there might be cancellations with higher order artifacts. We illustrate that this is indeed the case in this work, demonstrating the possible complicated dependence of observables on the lattice spacing and showing the intrinsic $\mathcal{O}(a)$ improvement of the SLiNC action. Since the $\mathcal{O}(g^2a^2)$ artifacts cannot be trustworthy for the whole range of employed momenta, it is unnatural to subtract them from the nonperturbative estimates.

As opposed to performing a Taylor expansion with respect to a and isolating the $\mathcal{O}(g^2a^2)$ terms, one may keep a finite everywhere and thus evaluate the lattice artifacts at one-loop order completely, proceeding as

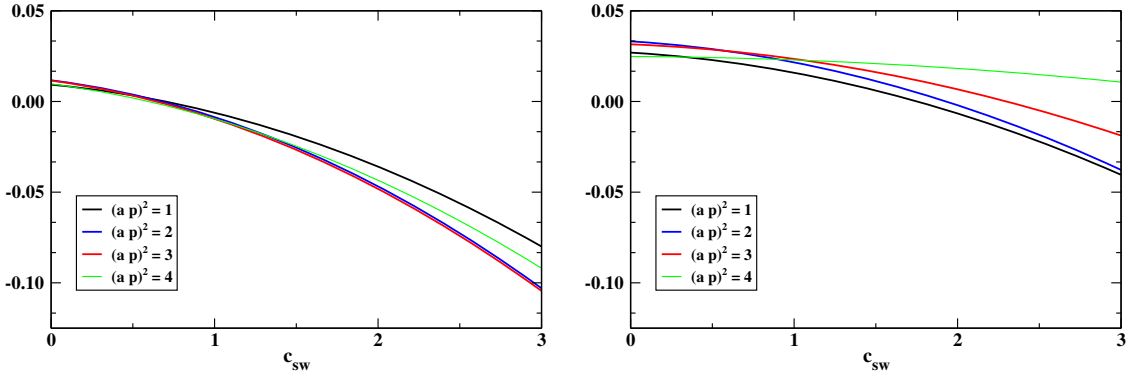

FIG. 4 (color online). $\Lambda_q^{(2)}$ as a function of $c_{\rm sw}$ for $\omega = 0.1$ and for representative values of diagonal $[(a\,p)/2(1,1,1,1)$, left] and nondiagonal momenta $[(a\,p,0,0,0)$, right].

follows: we denote by $F(p,a)$ the total one-loop correction—including $g^2 C_F/(16\pi^2)$—and by $\tilde{F}(p,a)$ the expression resulting from $F(p,a)$ by neglecting all contributions which vanish for $a \to 0$. Due to the nature of the computation to all orders in a, the dependence on the external momentum cannot be given in an analytic form for $F(p,a)$ since it is included in the propagators. Thus, we compute the one-loop expression separately for each value of the external momentum used in the simulations. From the latter expression one must omit the $\mathcal{O}(a^0)$ contributions $[\tilde{F}(p,a)]$; this is achieved by subtracting the $\mathcal{O}(g^2 a^0)$ terms, computed analytically in Sec. III A [Eqs. (16)–(21)]. Thus, the difference

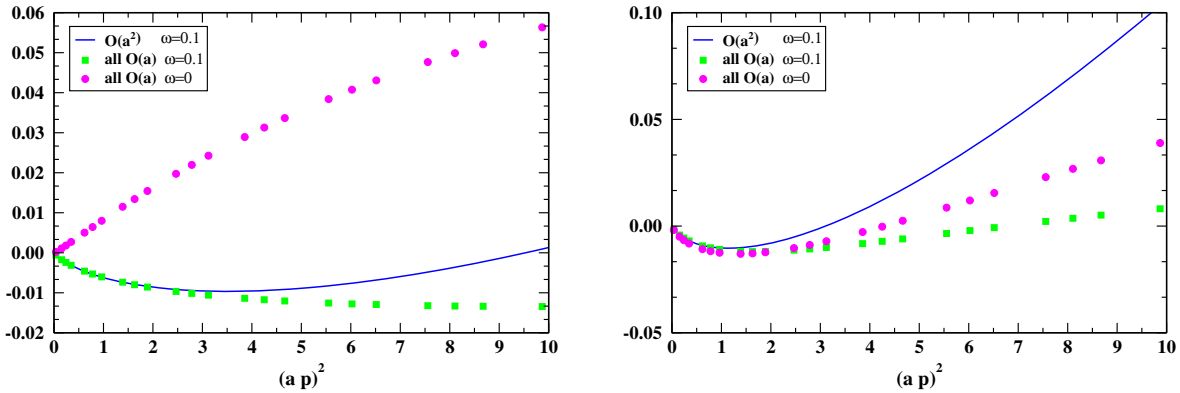

FIG. 5 (color online). Terms of all $\mathcal{O}(a)$ and $\mathcal{O}(a^2)$ for Z_q (left) and Z_T (right) as a function of $(a\,p)^2$.

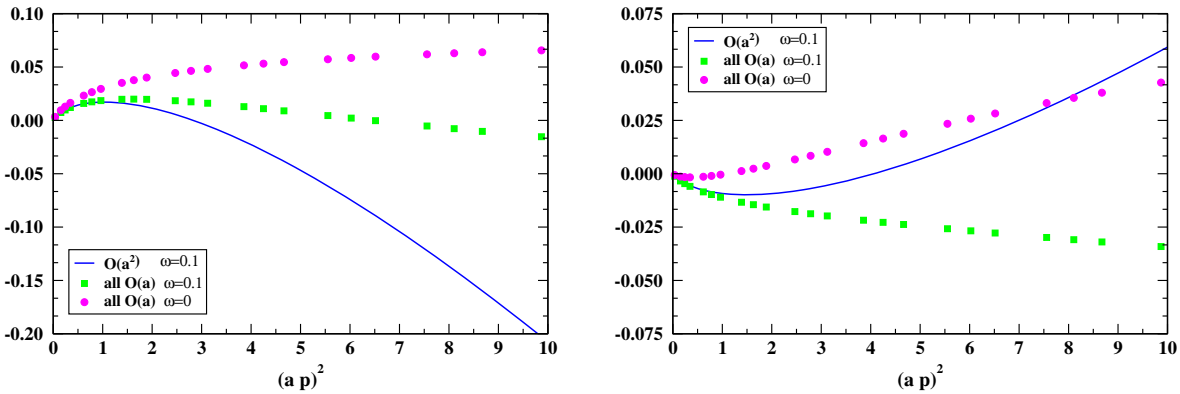

FIG. 6 (color online). Similar to Fig. 5 for Z_S (left) and Z_P (right).

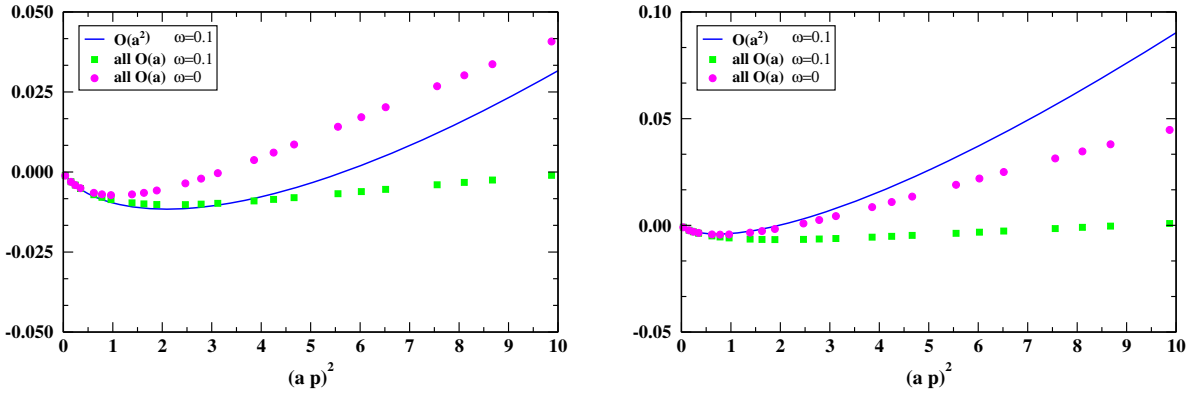

FIG. 7 (color online). Similar to Fig. 5 for Z_V (left) and Z_A (right).

$$D(p,a) = F(p,a) - \tilde{F}(p,a) \tag{25}$$

corresponds to the lattice artifacts in one-loop perturbation theory and is used to correct the discretization errors from the nonperturbative estimates (NP), as appears in Sec. V B:

$$Z^{\mathrm{RI'\text{-}MOM}}_{\mathrm{bare}}(p,a)_{\mathrm{NP,sub}} = Z^{\mathrm{RI'\text{-}MOM}}_{\mathrm{bare}}(p,a)_{\mathrm{NP}} - D(p,a). \tag{26}$$

One of the novelties of this work, as compared to Ref. [4], is that we have improved our codes for the computation of the one-loop diagrams in order to encompass more complicated actions, as in the present case. In fact, we are now in a position to compute the complete one-loop lattice artifacts for all actions appearing in the literature.

It is interesting to compare the $\mathcal{O}(a^2)$ terms and the total one-loop lattice artifacts, and thus we plot the two contributions in Figs. 5–7 for $c_{\mathrm{sw}} = 1$, and for two values of the stout parameter, $\omega = 0, 0.1$. For both $\omega = 0$ and $\omega = 0.1$ we use the tree-level Symanzik gluon action. To match our nonperturbative computation we choose diagonal momenta. A comparison of the lattice artifacts to all orders in a for $\omega = 0$ and $\omega = 0.1$ and for $1 < (a\,p)^2 < 10$ (which is the range of interest) confirms that the presence of the stout parameter suppresses them. An exception of this is Z_P for which both $\omega = 0$ and $\omega = 0.1$ are of the same order but go either direction of zero. Concentrating on $\omega = 0.1$, one observes that for small values of $(a\,p)^2$ the two computations (blue line, green points) lead to compatible results, as expected. The $\mathcal{O}(a^2)$ contribution increases with $(a\,p)^2$, while the complete one-loop artifacts are much smaller (except for Z_q and Z_P). It is worth mentioning that a similar test using $\omega = 0, 0.1$ and Wilson gluons has shown also similar behavior with the $\omega = 0.1$ terms to be suppressed compared to the $\omega = 0$ case. According to the authors' understanding this is an indication of artifacts' suppression as compared to the case presented in Ref. [4]—with $N_f = 2$ Wilson gluons—presumably due to the improvement of the action using the stout smearing.

IV. NONPERTURBATIVE RESULTS

We shall present our raw results now, including the extrapolation to the chiral limit, the conversion to the $\overline{\mathrm{MS}}$ scheme and subtraction of the pion pole in case of the pseudoscalar density.

A. RI′-MOM and chiral extrapolation

In Fig. 8 we show Z_q, Z_S, Z_V, Z_A, and Z_T as a function of the renormalization scale for our various pion masses. To see more clearly the dependence on the pion mass we take, as an example, the momentum $(a\,p)^2 \sim 2.5$, which is

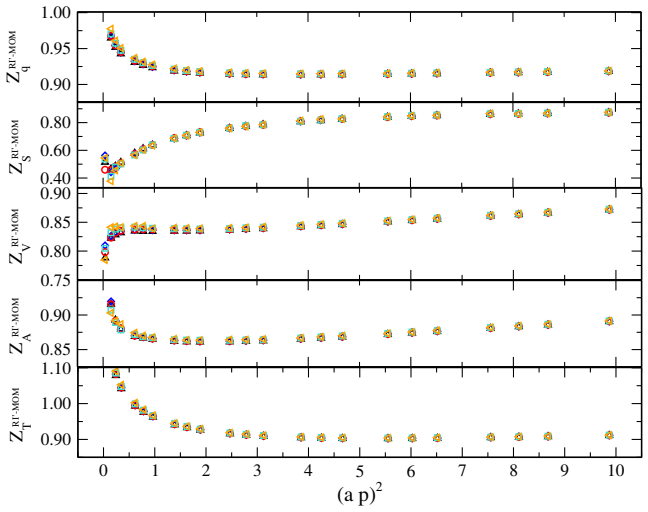

FIG. 8 (color online). Results on the Z-factors for all pion masses versus the renormalization scale in lattice units. Different colors and shapes denote different ensembles (see also legend of Fig. 9): black up triangles, blue diamonds, red circles, green squares, and yellow left triangles stand for $m_\pi = 465$, 439, 402, 345, and 290 MeV, respectively.

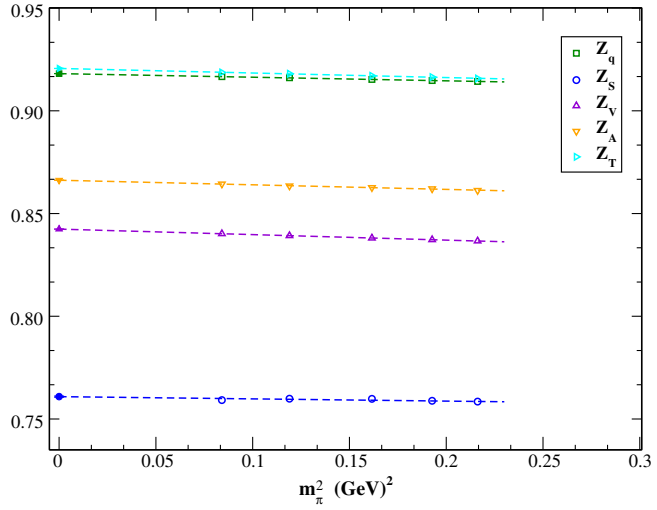

FIG. 9 (color online). The dependence of the Z-factors on the pion mass at $(ap)^2 \sim 2.5$, together with a linear fit.

within the range that we will fit the Z-factors. This dependence is found to be very weak, as shown in Fig. 9 for a particular value of the scale, and well represented by a linear curve. All other scales show a similar behavior. In the following we extrapolate the Z-factors linearly to the chiral limit for each value of $(ap)^2$. The Z-factor of the pseudoscalar density, Z_P, needs to be treated separately, because it suffers from the pion pole in the Green's function of Eq. (1). This we will deal with in Sec. IV C.

B. Conversion to $\overline{\text{MS}}$

Although RI′-MOM is a convenient scheme to compute the renormalization factors, our aim is to present them in the $\overline{\text{MS}}$ scheme. Starting from the results in RI′-MOM at various scales, μ, we convert them to the $\overline{\text{MS}}$ scheme at a reference scale; we will set that scale to 2 GeV. The conversion factors do not depend on the regularization scheme (and, thus, they are independent of the lattice discretization) when expressed in terms of the renormalized coupling constant. However, expressing them in terms of the bare coupling constant introduces a dependence on the action. The conversion factors, $C_{\mathcal{O}}^{\text{RI}'\text{-MOM},\overline{\text{MS}}}$, and the expression for running the scale to 2 GeV in $\overline{\text{MS}}$, $R(\mu, 2\text{ GeV})$, are defined such that:

$$Z_{\mathcal{O}}^{\overline{\text{MS}}}(2\text{ GeV}) = R(\mu, 2\text{ GeV})\, C_{\mathcal{O}}^{\text{RI}'\text{-MOM},\overline{\text{MS}}}\, Z_{\mathcal{O}}^{\text{RI}'\text{-MOM}}(\mu), \tag{27}$$

and their perturbative expressions are available up to three loops. For the relation between the renormalized coupling constant, g_R, and the bare one, g: $g_R = Z_g^{-1} g$, we use the two-loop results of Ref. [15] for Z_g corresponding to clover fermions and Wilson gluons. $R(\mu, 2\text{ GeV})$ is expressed in terms of $\Lambda_{\overline{\text{MS}}}$ which for $N_f = 3$ was estimated to be 339 MeV [16]. The conversion factors we use are adapted from Ref. [17] and are applicable to the naive dimensional regularization (NDR) of the $\overline{\text{MS}}$ scheme [18], in which $C_P = C_S$. Moreover, the conversion factor from the RI′-MOM to the $\overline{\text{MS}}$ scheme for the vector and axial-vector operators is 1.

In an alternative procedure the RGI scheme is used as an intermediate scheme to obtain the conversion factors for the operators. Those factors $C^{\text{RI}'\text{-MOM},\overline{\text{MS}}}$ are found from relating the renormalization function in $\overline{\text{MS}}$ (at 2 GeV) and RI′-MOM (at a scale μ):

$$\begin{aligned} Z_{\mathcal{O}}^{\text{RGI}} &= Z_{\mathcal{O}}^{\overline{\text{MS}}}(2\text{ GeV})\, \Delta Z_{\mathcal{O}}^{\overline{\text{MS}}}(2\text{ GeV}) \\ &= Z_{\mathcal{O}}^{\text{RI}'\text{-MOM}}(\mu)\, \Delta Z_{\mathcal{O}}^{\text{RI}'\text{-MOM}}(\mu), \end{aligned} \tag{28}$$

and thus

$$\begin{aligned} Z_{\mathcal{O}}^{\overline{\text{MS}}}(2\text{ GeV}) &= C_{\mathcal{O},\text{RGI}}^{\text{RI}'\text{-MOM},\overline{\text{MS}}}(\mu, 2\text{ GeV}) \\ &\quad \times Z_{\mathcal{O}}^{\text{RI}'\text{-MOM}}(\mu), \\ C_{\mathcal{O},\text{RGI}}^{\text{RI}'\text{-MOM},\overline{\text{MS}}}(\mu, 2\text{ GeV}) &= \frac{\Delta Z_{\mathcal{O}}^{\text{RI}'\text{-MOM}}(\mu)}{\Delta Z_{\mathcal{O}}^{\overline{\text{MS}}}(2\text{ GeV})}. \end{aligned} \tag{29}$$

The quantity $\Delta Z_{\mathcal{O}}^{S}(\mu)$ in scheme S is expressed in terms of the β-function and the anomalous dimension of the operator under study, $\gamma_{\mathcal{O}}^{S} \equiv \gamma^{S}$:

$$\begin{aligned} \Delta Z_{\mathcal{O}}^{S}(\mu) &= \left(2\beta_0 \frac{g^S(\mu)^2}{16\pi^2}\right)^{-\frac{\gamma_0}{2\beta_0}} \\ &\quad \times \exp\left\{\int_0^{g^S(\mu)} \mathrm{d}g' \left(\frac{\gamma^S(g')}{\beta^S(g')} + \frac{\gamma_0}{\beta_0 g'}\right)\right\}. \end{aligned} \tag{30}$$

To three-loop approximation $\Delta Z_{\mathcal{O}}^{S}(\mu)$ takes the form

$$\begin{aligned} \Delta Z_{\mathcal{O}}^{S}(\mu) &= \left(2\beta_0 \frac{g^S(\mu)^2}{16\pi^2}\right)^{-\frac{\gamma_0}{2\beta_0}} \left(1 + \frac{g^S(\mu)^2}{16\pi^2} \frac{\beta_1\gamma_0 - \beta_0\gamma_1^S}{2\beta_0^2} \right. \\ &\quad \left. + \frac{g^S(\mu)^4}{(16\pi^2)^2} \frac{-2\beta_0^3\gamma_2^S + \beta_0^2(\gamma_1^S(2\beta_1 + \gamma_1^S) + 2\beta_2\gamma_0) - 2\beta_0\beta_1\gamma_0(\beta_1 + \gamma_1^S) + \beta_1^2\gamma_0^2}{8\beta_0^4}\right). \end{aligned} \tag{31}$$

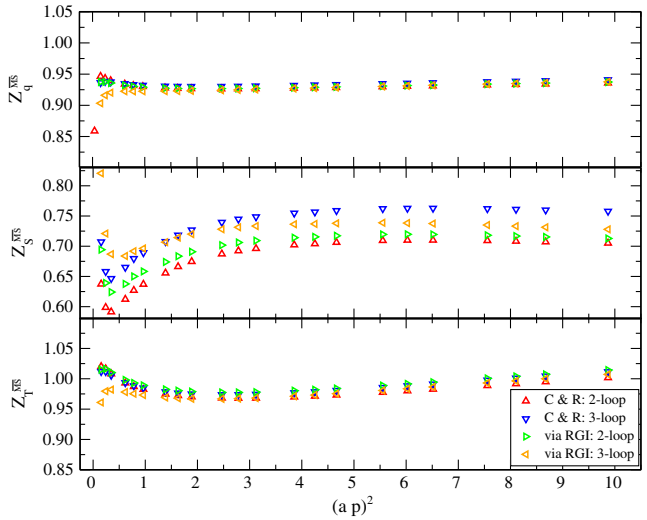

FIG. 10 (color online). $Z_q^{\overline{\rm MS}}$, $Z_S^{\overline{\rm MS}}$, $Z_T^{\overline{\rm MS}}$ ($m_\pi = 465$ MeV) using two-loop (red up triangles) and three-loop (blue down triangles) expressions for $C_{\mathcal{O}}^{\text{RI}'\text{-MOM},\overline{\rm MS}} R(\mu, 2\text{ GeV})$. Green right triangles (yellow left triangles) correspond to the two- (three-)loop expressions of Eq. (31) using the intermediate RGI scheme.

The expressions for the coupling $g^S(\mu)$ in the $\overline{\rm MS}$ and in the RI′-MOM schemes coincide to three loops and read [19]

$$\frac{g^S(\mu)^2}{16\pi^2} = \frac{1}{\beta_0 L} - \frac{\beta_1}{\beta_0^3}\frac{\log L}{L^2} + \frac{1}{\beta_0^5}\frac{\beta_1^2\log^2 L - \beta_1^2\log L + \beta_2\beta_0 - \beta_1^2}{L^3},$$
$$L = \log\frac{\mu^2}{\Lambda^2_{\overline{\rm MS}}}. \tag{32}$$

In Appendix B we give the definitions of the β-function and the anomalous dimension for the fermion field and local operators, as well as their perturbative coefficients to three loops. In Fig. 10 we demonstrate the effects in the Z-factors resulting from the use of the two- and three-loop expressions for $C_{\mathcal{O}}^{\text{RI}'\text{-MOM},\overline{\rm MS}}$ and $R(\mu, 2\text{ GeV})$, and the corresponding expressions for the alternative conversion (via RGI) as given by Eq. (31). The ensemble used for this figure corresponds to $m_\pi = 465$ MeV. We find that the discrepancies are at 8% maximum for Z_S (and consequently Z_P discussed later). For the standard conversion factors $C_{\mathcal{O}}^{\text{RI}'\text{-MOM},\overline{\rm MS}}$ the difference in the two-loop values of Z_g between the Wilson and tree-level Symanzik gluons is expected to be (based on their one-loop difference) within this systematic error. The conversion via the RGI scheme has the property that it uses continuum results; in the rest of the paper we use the intermediate RGI scheme and employ the three-loop result of Eq. (31) for all the conversions. In the final results presented in Sec. V we also give a systematic error due to differences in the conversion factor.

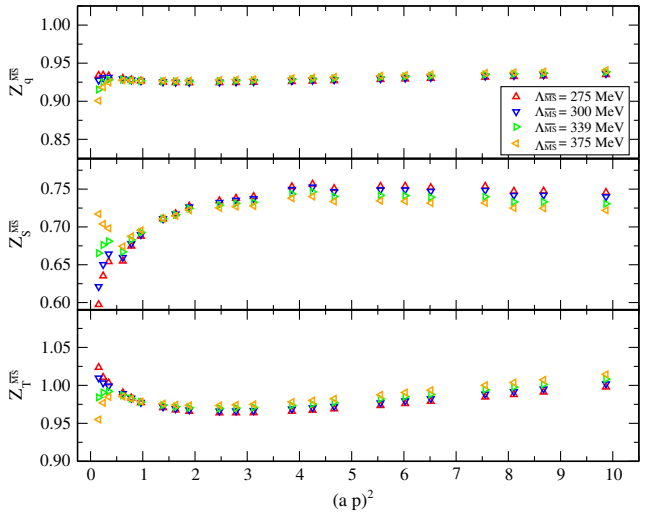

FIG. 11 (color online). Z_q, Z_S, Z_T in the $\overline{\rm MS}$ scheme using different values of $\Lambda_{\overline{\rm MS}}$.

Another systematic error could result from the ambiguity in the value of $\Lambda_{\overline{\rm MS}}$ needed in Eq. (32). Having this in mind, it is interesting to see how the conversion factors are affected by any variation of the value of $\Lambda_{\overline{\rm MS}}$. This is demonstrated in Fig. 11 using the three-loop expressions for the intermediate RGI scheme. We observed that the conversion factors of Z_q and Z_T are not affected by variations of $\Lambda_{\overline{\rm MS}}$. On the other hand, Z_S shows some sensitivity on $\Lambda_{\overline{\rm MS}}$ in the range of 275 to 375 MeV. Nevertheless, this dependence on $\Lambda_{\overline{\rm MS}}$ is smaller than the one due to the order of $g^S(\mu)$ used in the conversion factors.

C. Chiral extrapolation of Z_P and Z_P/Z_S

To obtain Z_P in the chiral limit, we must subtract the pion pole from the pseudoscalar vertex function $\Lambda_P(p, m_\pi)$. To do so we consider as ansatz a two-parameter fit function for each momentum p

$$f^{(2)}(p, m_\pi) = a_P(p) + \frac{c_P(p)}{m_\pi^2} \tag{33}$$

or a three-parameter fit function

$$f^{(3)}(p, m_\pi) = a_P(p) + b_P(p)m_\pi^2 + \frac{c_P(p)}{m_\pi^2}, \tag{34}$$

and fit Eq. (33) or Eq. (34) to the ratio

$$R(p, m_\pi) = \frac{\Lambda_P(p, m_\pi)}{Z_q(p, m_\pi)\, C_{P,\text{RGI}}^{\text{RI}'\text{-MOM},\overline{\rm MS}}(p, 2\text{ GeV})}. \tag{35}$$

The coefficient $a_P(p)$ is the number we are looking for, the continuum limit of which corresponds to $(Z_P^{\overline{\rm MS}})^{-1}$. In Fig. 12 we show the result of both local fits. The coefficient $b_P(p)$ turns out to be rather small. In fact, it is compatible

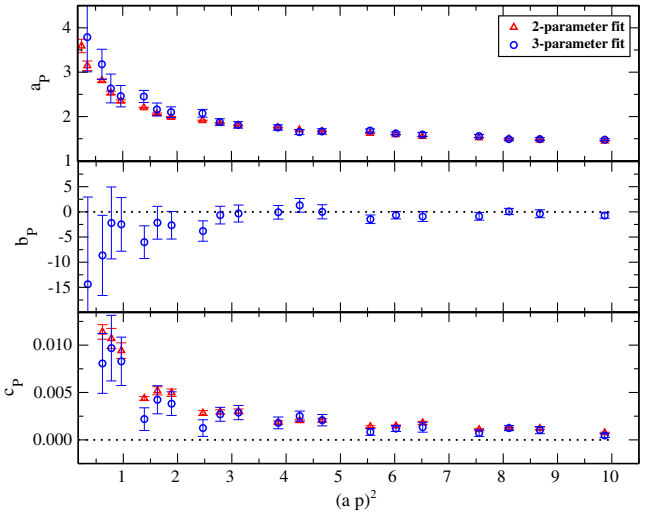

FIG. 12 (color online). Red triangles denote the parameters a_P, c_P extracted from the 2-parameter fit. Blue circles denote the parameters a_P, b_P, c_P extracted from the 3-parameter fit.

with zero. The two-parameter fit of Eq. (33) leads to significantly smaller errors on $a_P(p)$. In the following we shall employ the local two-parameter fit to subtract the pion pole and extrapolate Z_P to the chiral limit. The results will be shown in Sec. V. The stability of the fit is discussed in Appendix C using alternatives for the pion pole subtraction, along with an assessment of systematic errors.

In some applications a precise value of Z_P/Z_S is needed, which suggests a direct fit of the ratio. In this ratio the factors Z_q and $C_{\mathcal{O}}^{\mathrm{RI'\text{-}MOM},\overline{\mathrm{MS}}}$ drop out. To subtract the pion pole from $\Lambda_P(p, m_\pi)$, we proceed as before and fit Eq. (33) and Eq. (34), respectively, with coefficients $a_{PS}(p)$, $b_{PS}(p)$, and $c_{PS}(p)$ to

$$R(p, m_\pi) = \frac{\Lambda_P(p, m_\pi)}{\Lambda_S(p, m_\pi)}. \tag{36}$$

In the chiral limit $Z_S/Z_P = a_{PS}(p)$. Again, the parameter $b_{PS}(p)$ has little effect on the result. As before, we shall adopt the local two-parameter fit and show results of the continuum extrapolation in Sec. V.

V. CONTINUUM EXTRAPOLATIONS

We now come to the main topic of this paper, the subtraction of lattice artifacts. Clearly, the renormalization factors Z_V, Z_A and $Z_S^{\overline{\mathrm{MS}}}$, $Z_P^{\overline{\mathrm{MS}}}$ and $Z_T^{\overline{\mathrm{MS}}}$ show some residual dependence on $(a\,p)^2$, which we will address now. The final aim is to extrapolate the data to $(a\,p)^2 = 0$.

A. Unsubtracted data

Let us first look at the raw data, extrapolated to the chiral limit and converted to the $\overline{\mathrm{MS}}$ scheme in Sec. IV. In Figs. 13 and 14 we plot Z_V, Z_A and Z_P/Z_S as a function of $(a\,p)^2$. Similarly, in Figs. 15, 16, 17, and 18 we plot Z_q, Z_S, Z_P and

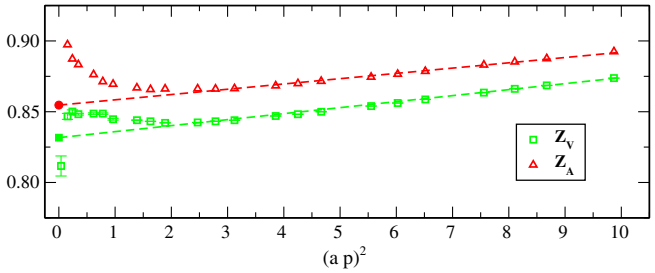

FIG. 13 (color online). The dependence of Z_V and Z_A on the renormalization scale, for the chirally extrapolated data. Dashed lines represent the continuum extrapolation and filled points the extrapolated value.

Z_T in the RI′-MOM and $\overline{\mathrm{MS}}$ scheme, respectively, at $\mu = 2$ GeV. We find Z_V, Z_A and Z_P/Z_S and $Z_S^{\overline{\mathrm{MS}}}$, $Z_P^{\overline{\mathrm{MS}}}$ and $Z_T^{\overline{\mathrm{MS}}}$ to lie approximately on a linear curve for $(a\,p)^2 \gtrsim 2$, which allows a fit to a straight line. The dashed lines show a fit to the interval $(a\,p)^2 \in [2, 10]$.

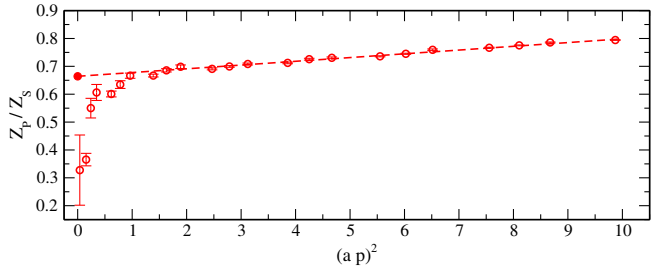

FIG. 14 (color online). Similar to Fig. 13 for Z_P.

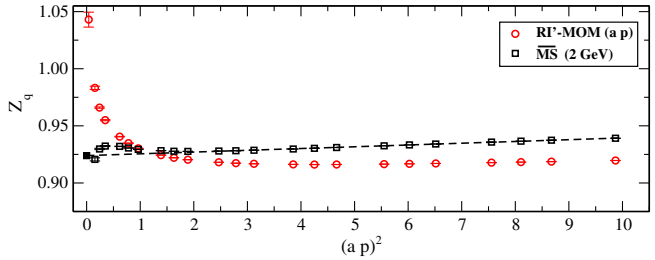

FIG. 15 (color online). The dependence of $Z_q^{\mathrm{RI'\text{-}MOM}}$ and $Z_q^{\overline{\mathrm{MS}}}$ on the momentum scale, for the chirally extrapolated nonperturbative data. Dashed lines represent the continuum extrapolation and filled points the extrapolated value.

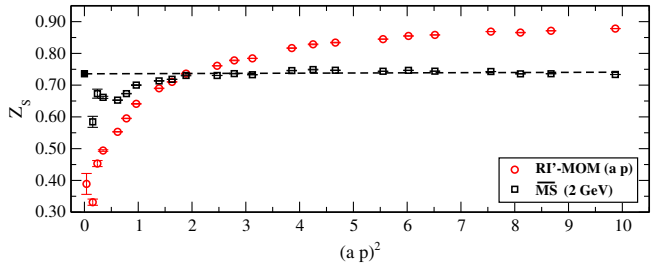

FIG. 16 (color online). Similar to Fig. 15 for Z_S.

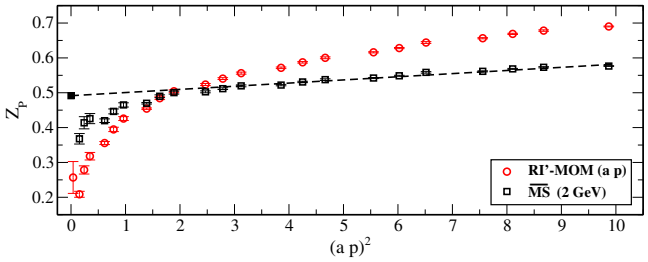

FIG. 17 (color online). Similar to Fig. 15 for Z_P.

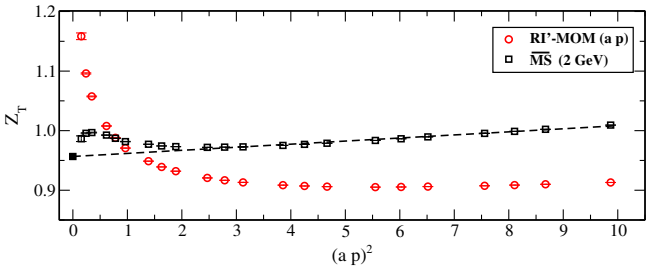

FIG. 18 (color online). Similar to Fig. 15 for Z_T.

While statistical errors are small, there are some systematic errors, which should be carefully examined. One source of error is the accuracy of the conversion factors. Another source arises from the choice of fit interval. We have also used various intervals for the fit, by shifting the upper and lower limits. The difference in results between the intervals [2, 10] and [2, 6] will give us an estimate of the systematic error.

In Table IV we present the Z-factors, after chiral and continuum extrapolation, from a fit to the interval $(a\,p)^2 \in [2, 10]$. The number in the first bracket indicates the purely statistical error. The number in the second bracket states the systematic error, which is taken from the difference of the fit to $(a\,p)^2 \in [2, 10]$ and [2, 6]. The third number, wherever it applies, reflects the difference of two- and three-loop conversion factors.

B. Subtraction of one-loop perturbative lattice artifacts

We now turn to the subtraction of lattice artifacts. There are two kinds of subtractions we employ (see Sec. III): the subtraction of one-loop $\mathcal{O}(a^2)$ corrections and the complete subtraction of one-loop lattice artifacts. For each case we use both the bare, g, and boosted coupling,

$$g_b^2 = \frac{g^2}{P(g)}, \tag{37}$$

where $P(g)$ is the plaquette at $\beta = 5.50$ and for the ensembles used in this work we find: $P(\beta = 5.5) \sim 0.52$. For the improvement coefficient $c_{\rm sw}$ we take the tree-level value, $c_{\rm sw} = 1$. The effect of the subtraction is demonstrated as examples in Figs. 19–21 for the chirally extrapolated data. For Z_q (Fig. 19) we find no clear preference for any kind of subtraction. In case of the quark-bilinear operators (Figs. 20 and 21) the $\mathcal{O}(g^2a^2)$ corrections are very small for $(a\,p)^2 < 4$, but beyond that they get out of control and show significant $O((a\,p)^4)$ effects. Complete subtraction of one-loop lattice artifacts,

TABLE IV. Continuum extrapolated values on $Z_q^{\overline{\text{MS}}}$, $Z_S^{\overline{\text{MS}}}$, $Z_P^{\overline{\text{MS}}}$, $Z_T^{\overline{\text{MS}}}$, Z_V, Z_A, and Z_P/Z_S. The number in the first (second) bracket is the statistical (systematic) error, and where applicable, the one in the third bracket comes from the difference in using the two- and three-loop results for the conversion factor via RGI.

$Z_q^{\overline{\text{MS}}}$ (2 GeV)	0.9239(001)(003)(028)
$Z_S^{\overline{\text{MS}}}$ (2 GeV)	0.7356(053)(155)(277)
$Z_P^{\overline{\text{MS}}}$ (2 GeV)	0.4915(025)(125)(184)
Z_P/Z_S	0.6643(032)(023)
Z_V	0.8317(005)(021)
Z_A	0.8547(008)(036)
$Z_T^{\overline{\text{MS}}}$ (2 GeV)	0.9566(013)(054)(101)

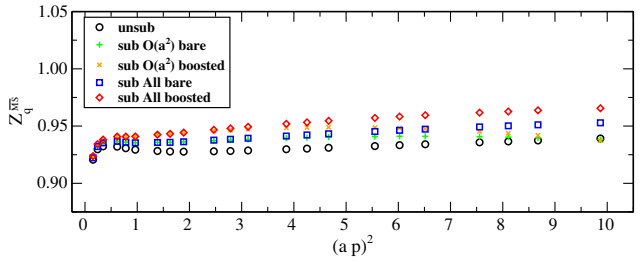

FIG. 19 (color online). Chirally extrapolated values for $Z_q^{\overline{\text{MS}}}$ before the perturbative subtraction (black circles) and after subtraction of (a) $\mathcal{O}(g^2a^2)$ terms using bare coupling, g (green plus points), (b) $\mathcal{O}(g_b^2a^2)$ terms using boosted coupling, g_b (orange crosses), (c) complete subtraction using g (blue squares), and (d) complete subtraction using g_b (red diamonds).

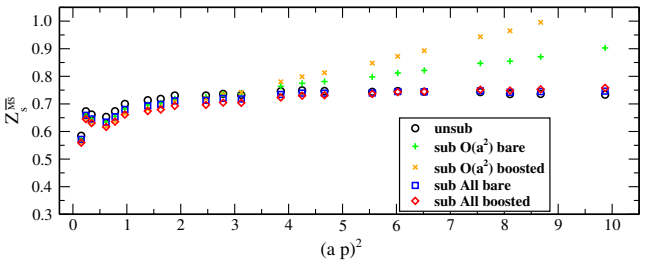

FIG. 20 (color online). Similar to Fig. 19 for Z_S.

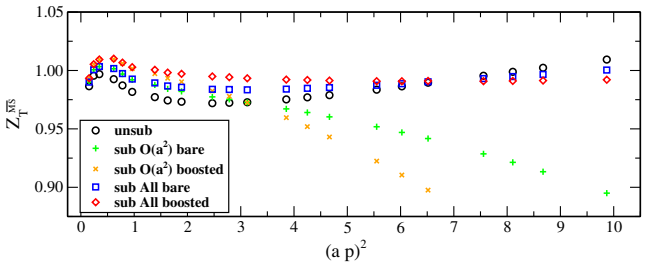

FIG. 21 (color online). Similar to Fig. 19 for Z_T.

on the other hand, has a small, albeit appreciable, effect on the Z-factors. In case of Z_V, Z_A (not shown here) and Z_T the data is brought on a perfectly straight line for $(a\,p)^2 \in [2, 10]$, using the boosted coupling g_b^2.

VI. FINAL RESULTS AND DISCUSSION

We take the lattice data of Sec. IV, improved by complete subtraction of one-loop lattice artifacts with boosted coupling g_b, as our final result. In Figs. 22–28 we show the Z-factors before and after the subtraction, together with a linear extrapolation to the continuum.

In Table V we give our final numbers, corresponding to the solid diamonds in Figs. 22–28. The corrected numbers differ by up to 8% from the unsubtracted results in Table IV. As can be seen in both Tables IV and V the errors due to the choice of the fit interval ([2, 10] and [2:6]) are much larger than the statistical errors. It measures the influence of the larger scales (ap) to the final values of the renormalization factors.

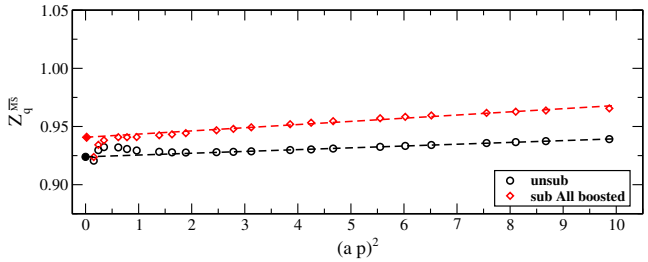

FIG. 22 (color online). Chirally extrapolated values for $Z_q^{\overline{\rm MS}}$ prior the perturbative subtraction (black circles) and after the complete subtraction of one-loop lattice artifacts using g_b (red diamonds).

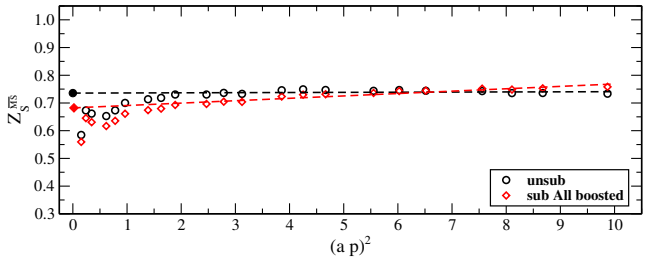

FIG. 23 (color online). Similar to Fig. 22 for Z_S.

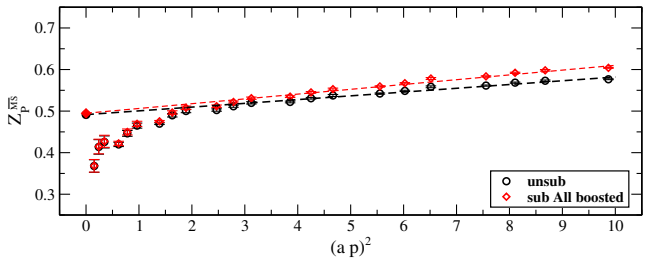

FIG. 24 (color online). Similar to Fig. 22 for Z_P.

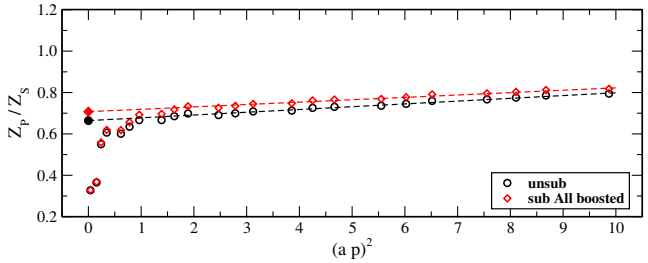

FIG. 25 (color online). Similar to Fig. 22 for Z_P/Z_S.

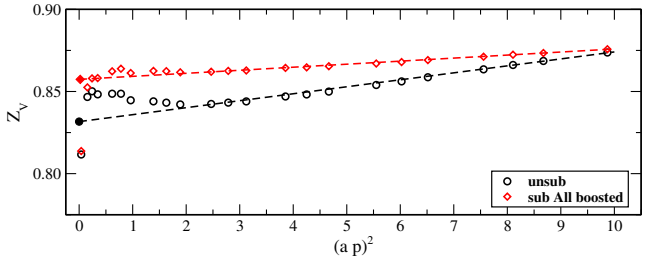

FIG. 26 (color online). Similar to Fig. 22 for Z_V.

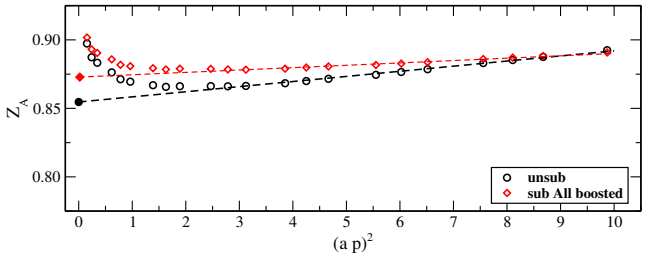

FIG. 27 (color online). Similar to Fig. 22 for Z_A.

The conversion factors to the RGI scheme and the RI′-MOM scheme at $\mu = 1/a$ are given by

$$
\begin{aligned}
Z_q^{\rm RGI} &= 0.9461 Z_q^{\overline{\rm MS}}, & Z_q^{\rm RI'\text{-}MOM} &= 1.0004 Z_q^{\overline{\rm MS}},\\
Z_S^{\rm RGI} &= 0.7503 Z_S^{\overline{\rm MS}}, & Z_S^{\rm RI'\text{-}MOM} &= 0.9211 Z_S^{\overline{\rm MS}},\\
Z_P^{\rm RGI} &= 0.7503 Z_P^{\overline{\rm MS}}, & Z_P^{\rm RI'\text{-}MOM} &= 0.9211 Z_P^{\overline{\rm MS}},\\
Z_T^{\rm RGI} &= 1.0604 Z_T^{\overline{\rm MS}}, & Z_T^{\rm RI'\text{-}MOM} &= 0.9870 Z_T^{\overline{\rm MS}}.
\end{aligned}
\tag{38}
$$

To recapitulate, in a previous work [4] we have computed renormalization factors of quark-bilinear operators for $N_f = 2$ flavors of dynamical clover fermions. We have

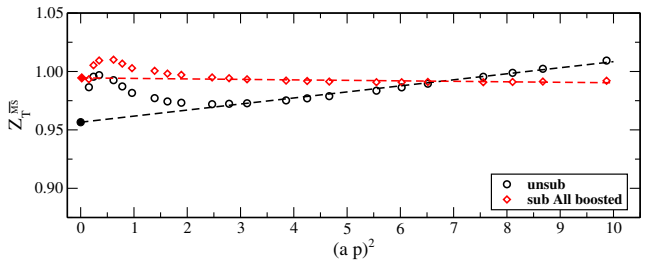

FIG. 28 (color online). Similar to Fig. 22 for Z_T.

TABLE V. Continuum results for Z_q, Z_S, Z_P, Z_P/Z_S, Z_V, Z_A, and Z_T in the $\overline{\text{MS}}$ scheme at $\mu = 2$ GeV, where it applies. The numbers refer to the fit interval $(a\,p)^2 \in [2, 10]$. The first number in brackets is the statistical error, the second number the systematic error due to the fit range.

$Z_q^{\overline{\text{MS}}}$	0.9408(008)(024)
$Z_S^{\overline{\text{MS}}}$	0.6822(061)(176)
$Z_P^{\overline{\text{MS}}}$	0.4948(026)(128)
Z_P/Z_S	0.7075(036)(068)
Z_V	0.8574(002)(007)
Z_A	0.8728(006)(027)
$Z_T^{\overline{\text{MS}}}$	0.9945(010)(035)

refined the original procedure [1] in several aspects, including the use of momentum sources and the perturbative subtraction of lattice artifacts. In this work we extended the calculation to $N_f = 3$ flavors of SLiNC fermions [6]. Using twisted boundary conditions, the lattice momenta were chosen to lie strictly on the diagonal, $p_\mu = \sqrt{p^2/4}, \forall \mu$.

Complete subtraction of one-loop lattice artifacts has brought Z_V, Z_A, $Z_S^{\overline{\text{MS}}}$, $Z_P^{\overline{\text{MS}}}$, and $Z_T^{\overline{\text{MS}}}$ onto a straight line for $(a\,p)^2 \in [2, 10]$,

$$Z(p) = Z(0) + Z'(0)(a\,p)^2, \tag{39}$$

with the continuum value being given by $Z(0)$.[1] The corrections are found to be substantial. In case of Z_S they amount to 8%. The renormalization factor of the local vector current, Z_V, can be determined independently from the Dirac form factor of the proton at zero momentum transfer by enforcing charge conservation. In [21] we found $Z_V = 0.857(1)$ at a pion mass of $m_\pi = 220$ MeV, which is in perfect agreement with our final number in Table V. This gives support for our procedure of subtracting lattice artifacts.

It helped that the unsubtracted data were approximately linear in $(a\,p)^2$ already for $(a\,p)^2 \gtrsim 2$, in contrast to the case of $N_f = 2$ flavors of clover fermions and the plaquette action [4]. We attribute that to the Symanzik and stout-link improved action employed here, which appears to suppress lattice artifacts in quark Green's functions; see e.g., Figs. 5–7 demonstrating that the stout smearing leads to smaller lattice artifacts compared to the nonsmeared case ($\omega = 0$).

ACKNOWLEDGMENTS

The numerical configuration generation was performed using the BQCD lattice QCD program, [22], on the IBM BlueGeneQ using DIRAC 2 resources (EPCC, Edinburgh, UK), the BlueGene P and Q at NIC (Jülich, Germany) and the Cray XC30 at HLRN (Berlin and Hannover, Germany). The BlueGene codes were optimized using Bagel [23]. The Chroma software library [24] was used in the data analysis. This work has been supported in part by the European Grants No. 227431 (Hadron Physics2), No. 283286 (HadronPhysics3), and by the Australian Research Council under Grants No. FT100100005 and No. DP140103067 (J. M. Z.). Further support was provided by the project TECHNOLOGY/ΘΕΠΙΣ/0311(BE)/16 funded by the Cyprus Research Promotion Foundation, and by Deutsche Forschungsgemeinschaft DFG Grant under Contract No. SCHI 422/9-1.

APPENDIX A: PERTURBATIVE RESULTS

In this section we summarize the perturbative results for the $\mathcal{O}(g^2a^2)$ contributions $\Lambda_q^{(2)}$ and $\Lambda_{\mathcal{O}}^{(2)}$ as defined in Sec. III [see Eq. (22)]. For simplicity, we restrict our study to the case of the SLiNC action, which uses tree-level Symanzik gluons. The expressions, evaluated at $\omega = 0$, correspond to the usual clover action. Our results are given as a function of the momentum p and general values for the action parameters c_{sw}, ω. The gauge fixing parameter α is 0 (1) for the Landau (Feynman) gauge:

$$\begin{aligned}\Lambda_q^{(2)} = a^2\frac{g^2C_F}{16\pi^2}\Bigg(p^2\Bigg(&1.14717 - 1.51605\alpha + c_{\text{sw}}(-0.653431 + 0.505886\omega) - 0.497834c_{\text{sw}}^2\\ &- 12.0983\omega + 28.0799\omega^2 + \log(a^2p^2)\left(-\frac{73}{360} + \frac{3\alpha}{8} + \frac{c_{\text{sw}}^2}{4} + \frac{c_{\text{sw}}}{4} + \omega\right)\Bigg)\\ &+ \frac{p4}{p^2}\Bigg(2.10650 + 0.395834\alpha + c_{\text{sw}}(0.284537 - 0.362507\omega) + 0.128381c_{\text{sw}}^2\\ &- 4.08165\omega - 16.0889\omega^2 - \frac{157}{180}\log(a^2p^2)\Bigg)\Bigg),\end{aligned} \tag{A1}$$

[1] Although the explicit chiral symmetry breaking leads to $\mathcal{O}(a\,p)$ terms in the Green's functions, these terms always have the opposite chirality to the Born term, so they do not contribute to the trace we are fitting to, which justifies the absence of these terms in our fit procedure. For instance, the one-loop expressions for Λ_A in Appendix A.4 of Ref. [20] show that there is indeed an $\mathcal{O}(a\,p)$ term, but it has the Dirac structure $ai(\not{p}\gamma_\mu\gamma_5 + \gamma_\mu\gamma_5\not{p})$ and so it has no contribution to the trace which we plot. Looking at the other operators, we see that this is a general result, the $\mathcal{O}(a\,p)$ terms are always killed by tracing with the Born term.

$$\Lambda_S^{(2)} = a^2\frac{g^2C_F}{16\pi^2}\left(p^2\left(-1.20757 + 0.75755\alpha + c_{\rm sw}(3.19935 - 4.79168\omega) - 0.69430c_{\rm sw}^2 - 0.64987\omega + 0.71144\omega^2 + \log(a^2p^2)\left(\frac{17}{360} - \frac{3\alpha}{8} - \frac{5c_{\rm sw}}{4} + \frac{c_{\rm sw}^2}{4} + \omega\right)\right) + \frac{p4}{p^2}\left(1.6065 + 0.52083\alpha + c_{\rm sw}(0.28454 - 0.36251\omega) + 0.12838c_{\rm sw}^2 - 4.08165\omega - 16.0889\omega^2 - \frac{157}{180}\log(a^2p^2)\right)\right), \tag{A2}$$

$$\Lambda_P^{(2)} = a^2\frac{g^2C_F}{16\pi^2}\left(p^2\left(0.44076 - 0.67794\alpha + c_{\rm sw}(0.50589\omega - 0.65343) - 0.22227c_{\rm sw}^2 - 5.59237\omega - 1.17320\omega^2 + \log(a^2p^2)\left(\frac{17}{360} + \frac{\alpha}{8} + \frac{c_{\rm sw}}{4} + \frac{c_{\rm sw}^2}{4} + \omega\right)\right) + \frac{p4}{p^2}\left(1.6065 + 0.52083\alpha + c_{\rm sw}(0.28454 - 0.36251\omega) + 0.12838c_{\rm sw}^2 - 4.08165\omega - 16.0889\omega^2 - \frac{157}{180}\log(a^2p^2)\right)\right), \tag{A3}$$

$$\Lambda_V^{(2)} = a^2\frac{g^2C_F}{16\pi^2}\left(p^2\left(0.44724 - 0.79717\alpha + c_{\rm sw}(1.83028\omega - 1.61663) - 0.14183c_{\rm sw}^2 - 1.02045\omega + 1.46637\omega^2 + \log(a^2p^2)\left(\frac{47}{360} + \frac{3\alpha}{16} + \frac{5c_{\rm sw}}{8} - \frac{c_{\rm sw}^2}{8} - \frac{\omega}{2}\right)\right) + \frac{p4}{p^2}\left(2.54053 + 0.23958\alpha + c_{\rm sw}(0.28454 - 0.36251\omega) + 0.12838c_{\rm sw}^2 - 4.08165\omega - 16.0889\omega^2 - \frac{157}{180}\log(a^2p^2)\right)\right), \tag{A4}$$

$$\Lambda_A^{(2)} = a^2\frac{g^2C_F}{16\pi^2}\left(p^2\left(-0.37692 - 0.07942\alpha + c_{\rm sw}(0.30976 - 0.81851\omega) - 0.85384c_{\rm sw}^2 + 1.45079\omega + 2.40868\omega^2 + \log(a^2p^2)\left(\frac{47}{360} - \frac{\alpha}{16} - \frac{c_{\rm sw}}{8} + \frac{5c_{\rm sw}^2}{8} - \frac{\omega}{2}\right)\right) + \frac{p4}{p^2}\left(2.54053 + 0.23958\alpha + c_{\rm sw}(0.28454 - 0.36251\omega) + 0.12838c_{\rm sw}^2 - 4.08165\omega - 16.0889\omega^2 - \frac{157}{180}\log(a^2p^2)\right)\right), \tag{A5}$$

$$\Lambda_T^{(2)} = a^2\frac{g^2C_F}{16\pi^2}\left(p^2\left(0.17468 - 0.59766\alpha + c_{\rm sw}(1.38881\omega - 1.29556) - 0.51102c_{\rm sw}^2 + 1.32727\omega + 2.66032\omega^2 + \log(a^2p^2)\left(\frac{19}{120} + \frac{\alpha}{8} + \frac{c_{\rm sw}}{2} + \frac{c_{\rm sw}^2}{4} - \omega\right)\right) + \frac{p4}{p^2}\left(2.85187 + 0.14583\alpha + c_{\rm sw}(0.28454 - 0.36251\omega) + 0.12838c_{\rm sw}^2 - 4.08165\omega - 16.0889\omega^2 - \frac{157}{180}\log(a^2p^2)\right)\right). \tag{A6}$$

APPENDIX B: β FUNCTION AND ANOMALOUS DIMENSIONS

In this appendix we give the definitions of the β-function and the anomalous dimension for the fermion field and the local operators. The perturbative coefficients up to three loops are given in $SU(3)$ and in the Landau gauge.

The scale dependence of the renormalized operator is encoded in the anomalous dimension and is defined as

$$\gamma^{\mathcal{S}} = -\mu\frac{\mathrm{d}}{\mathrm{d}\mu}\log Z_{\mathcal{S}} = \gamma_0\frac{g^{\mathcal{S}}(\mu)^2}{16\pi^2} + \gamma_1^{\mathcal{S}}\left(\frac{g^{\mathcal{S}}(\mu)^2}{16\pi^2}\right)^2 + \gamma_2^{\mathcal{S}}\left(\frac{g^{\mathcal{S}}(\mu)^2}{16\pi^2}\right)^3 + \cdots, \tag{B1}$$

where $\mathcal{S}$ is the renormalization scheme. The β-function is defined as

$$\beta^{\mathcal{S}} = \mu\frac{\mathrm{d}}{\mathrm{d}\mu}g^{\mathcal{S}}(\mu) = -\beta_0\frac{g^{\mathcal{S}}(\mu)^3}{16\pi^2} - \beta_1\frac{g^{\mathcal{S}}(\mu)^5}{(16\pi^2)^2} - \beta_2^{\mathcal{S}}\frac{g^{\mathcal{S}}(\mu)^7}{(16\pi^2)^3} + \cdots. \tag{B2}$$

The coefficients of the β-function in the $\overline{\mathrm{MS}}$ and the RI′-MOM schemes coincide up to three loops and are given by [17,25]

$$\beta_0 = 11 - \frac{2}{3}N_f, \tag{B3}$$

$$\beta_1 = 102 - \frac{38}{3}N_f, \tag{B4}$$

$$\beta_2 = \frac{2857}{2} - \frac{5033}{18}N_f + \frac{325}{54}N_f^2. \tag{B5}$$

The coefficients of the anomalous dimension for the quark field in the $\overline{\mathrm{MS}}$ and RI′-MOM schemes are [26]

$$\gamma_0 = 0, \tag{B6}$$

$$\gamma_1 = \frac{134}{3} - \frac{8}{3}N_f, \tag{B7}$$

$$\gamma_2^{\overline{\mathrm{MS}}} = \frac{20729}{18} - 79\zeta_3 - \frac{1100}{9}N_f + \frac{40}{27}N_f^2, \tag{B8}$$

$$\gamma_2^{\mathrm{RI'\text{-}MOM}} = \frac{52321}{18} - 79\zeta_3 - \frac{1100}{9}N_f + \frac{40}{27}N_f^2, \tag{B9}$$

for the scalar/pseudoscalar operators [27,28]:

$$\gamma_0 = -8, \tag{B10}$$

$$\gamma_1^{\overline{\mathrm{MS}}} = -\frac{404}{3} + \frac{40}{9}N_f, \tag{B11}$$

$$\gamma_1^{\mathrm{RI'\text{-}MOM}} = -252 + \frac{104}{9}N_f, \tag{B12}$$

$$\gamma_2^{\overline{\mathrm{MS}}} = -2498 + \left(\frac{4432}{27} + \frac{320}{3}\zeta_3\right)N_f + \frac{280}{81}N_f^2, \tag{B13}$$

$$\gamma_2^{\mathrm{RI'\text{-}MOM}} = -\frac{40348}{3} + \frac{6688}{3}\zeta_3 + \left(\frac{35176}{27} - \frac{256}{9}\zeta_3\right)N_f - \frac{1712}{81}N_f^2, \tag{B14}$$

($\zeta_3 = 1.20206\ldots$) and for the tensor [17,29]:

$$\gamma_0 = \frac{8}{3}, \tag{B15}$$

$$\gamma_1 = \frac{724}{9} - \frac{104}{27}N_f, \tag{B16}$$

$$\gamma_2^{\overline{\mathrm{MS}}} = \frac{105110}{81} - \frac{1856}{27}\zeta_3 - \left(\frac{10480}{81} + \frac{320}{9}\zeta_3\right)N_f - \frac{8}{9}N_f^2, \tag{B17}$$

$$\gamma_2^{\mathrm{RI'\text{-}MOM}} = \frac{359012}{81} - \frac{26144}{27}\zeta_3 + \left(-\frac{39640}{81} + \frac{512}{27}\zeta_3\right)N_f + \frac{2288}{243}N_f^2. \tag{B18}$$

APPENDIX C: AN ALTERNATIVE FOR THE PION POLE SUBTRACTION

Here we mention an alternative in handling the pion pole subtraction to determine the renormalization factors for Z_P. We can perform a global fit to the ratio of Eq. (35) taking into account the data at all pion masses and all scales simultaneously. Since in the same fit we combine both correlated and uncorrelated data extracted from different ensembles, we use the super-jackknife procedure [30] for the error estimation of the fit parameters. We employ a fit function with four, five, and six parameters, of the form

$$f^{(4)}(p, m_\pi) = a_0 + a_2p^2 + \frac{c_0 + c_2p^2}{m_\pi^2}, \tag{C1}$$

$$f^{(5)}(p, m_\pi) = a_0 + a_2p^2 + b_0m_\pi^2 + \frac{c_0 + c_2p^2}{m_\pi^2}, \tag{C2}$$

$$f^{(6)}(p, m_\pi) = a_0 + a_2p^2 + (b_0 + b_2p^2)m_\pi^2 + \frac{c_0 + c_2p^2}{m_\pi^2}. \tag{C3}$$

TABLE VI. Estimates for Z_P in the $\overline{\text{MS}}$ scheme using the global fits of Eqs. (C1)–(C3) and the data in the momentum range [2, 10]. Statistical errors are shown in parentheses.

	4-parameter fit	5-parameter fit	6-parameter fit
$Z_P^{\overline{\text{MS}}}$	0.4917(022)	0.4921(078)	0.4852(176)

In the above functions the parameters a_i, b_i, c_i are constants, but their estimation depends on the range of momenta that we take into account. Since the data at $(a\,p)^2 < 1$ do not exhibit any plateau behavior, they are entirely excluded from the fit. In fact, in the application of each fit shown in Eqs. (C1)–(C3), we use data corresponding to various momentum ranges, $(a\,p)^2$ (see text below). Similarly to the case of the two- and three-parameter fit, we are interested in extracting Z_P in $\overline{\text{MS}}$ with a single fit which is related to a_0, through $Z_P^{\overline{\text{MS}}} = (a_0)^{-1}$. To summarize, we have a total of 12 estimates for $Z_P^{\overline{\text{MS}}}$ extracted from the global fits, which correspond to all combinations between the three fit functions [Eqs. (C1)–(C3)] and the four momentum ranges in $(a\,p)^2 \in [1, 10]$, [2, 6], [2, 10], and [3.7, 10]. We find that the six-parameter fit is not very stable, while the four- and five-parameter global fits give compatible results with the local two- and three-parameter local fits applied to each momentum squared individually. An interesting observation is that the results obtained using the interval [2, 10] are compatible for all types of fits discussed here (see Table VI). The same global fitting has been tested to find Z_P/Z_S.

We find that the four-, five-, and six-parameter global fits are, in general, more unstable compared to the two- and three-parameter local fits and will not be used as final estimates. Moreover, the restriction of the global fitting functions to have quadratic dependence with respect to the momentum [Eqs. (C1)–(C3)] is not based on any theoretical arguments. Nevertheless, agreement within error bars between different fits gives confidence on the final estimate.

As a result of these studies, in Sec. V we have used the local two-parameter fit to remove the pion pole and combine it with a linear fit in the $(a\,p)^2$ interval [2, 10] counting for a remaining momentum dependence in the nonpole term after chiral extrapolation. The resulting constant is then the inverse of the renormalization function in the $\overline{\text{MS}}$ scheme.

[1] G. Martinelli, C. Pittori, C. T. Sachrajda, M. Testa, and A. Vladikas, Nucl. Phys. **B445**, 81 (1995).
[2] M. Göckeler, R. Horsley, Y. Nakamura, H. Perlt, D. Pleiter *et al.*, Phys. Rev. D **82**, 114511 (2010).
[3] M. Constantinou, V. Lubicz, H. Panagopoulos, and F. Stylianou, J. High Energy Phys. 10 (2009) 064.
[4] M. Constantinou, M. Costa, M. Göckeler, R. Horsley, H. Panagopoulos, H. Perlt, P. E. L. Rakow, G. Schierholz, and A. Schiller, Phys. Rev. D **87**, 096019 (2013).
[5] N. Cundy, M. Göckeler, R. Horsley, T. Kaltenbrunner, A. Kennedy *et al.*, Phys. Rev. D **79**, 094507 (2009).
[6] W. Bietenholz, V. Bornyakov, M. Göckeler, R. Horsley, W. Lockhart *et al.*, Phys. Rev. D **84**, 054509 (2011).
[7] M. Göckeler, R. Horsley, E.-M. Ilgenfritz, H. Perlt, P. E. Rakow, G. Schierholz, and A. Schiller, Phys. Rev. D **54**, 5705 (1996).
[8] M. Göckeler, R. Horsley, H. Oelrich, H. Perlt, D. Petters, P.E.L. Rakow, A. Schäfer, G. Schierholz, and A. Schiller, Nucl. Phys. **B544**, 699 (1999).
[9] M. Luscher, J. High Energy Phys. 08 (2010) 071.
[10] S. Borsanyi, S. Durr, Z. Fodor, C. Hoelbling, S. D. Katz *et al.*, J. High Energy Phys. 09 (2012) 010.
[11] R. Horsley, J. Najjar, Y. Nakamura, H. Perlt, D. Pleiter *et al.*, *Proc. Sci.*, LATTICE2013 (2013) 249.
[12] R. Arthur and P. Boyle (RBC Collaboration, UKQCD Collaboration), Phys. Rev. D **83**, 114511 (2011).
[13] R. Horsley, H. Perlt, P. Rakow, G. Schierholz, and A. Schiller, Phys. Rev. D **78**, 054504 (2008).
[14] C. Alexandrou, M. Constantinou, T. Korzec, H. Panagopoulos, and F. Stylianou, Phys. Rev. D **86**, 014505 (2012).
[15] A. Bode and H. Panagopoulos, Nucl. Phys. **B625**, 198 (2002).
[16] P. D. Group, J. Beringer *et al.*, Phys. Rev. D **86**, 010001 (2012).
[17] J. Gracey, Nucl. Phys. **B662**, 247 (2003).
[18] A. J. Buras and P. H. Weisz, Nucl. Phys. **B333**, 66 (1990).
[19] A. I. Alekseev, Few-Body Syst. **32**, 193 (2003).
[20] S. Capitani, M. Gockeler, R. Horsley, H. Perlt, P. E. Rakow, G. Schierholz, and A. Schiller, Nucl. Phys. **B593**, 183 (2001).
[21] P. E. Shanahan, R. Horsley, Y. Nakamura, D. Pleiter, P. E. L. Rakow, G. Schierholz, H. Stüben, A. W. Thomas, R. D. Young, and J. M. Zanotti, Phys. Rev. D **90**, 034502 (2014).
[22] Y. Nakamura and H. Stuben, *Proc. Sci.*, LATTICE2010 (2010) 040.
[23] P. A. Boyle, Comput. Phys. Commun. **180**, 2739 (2009).
[24] R. G. Edwards and B. Joo (SciDAC Collaboration, LHPC Collaboration, UKQCD Collaboration), Nucl. Phys. B, Proc. Suppl. **140**, 832 (2005).
[25] T. van Ritbergen, J. Vermaseren, and S. Larin, Phys. Lett. B **400**, 379 (1997).
[26] K. Chetyrkin and A. Retey, Nucl. Phys. **B583**, 3 (2000).
[27] K. Chetyrkin, Phys. Lett. B **404**, 161 (1997).
[28] J. Vermaseren, S. Larin, and T. van Ritbergen, Phys. Lett. B **405**, 327 (1997).
[29] J. Gracey, Phys. Lett. B **488**, 175 (2000).
[30] J. Bratt *et al.* (LHPC Collaboration), Phys. Rev. D **82**, 094502 (2010).